

Non-Hermitian Anharmonicity Induces Single-Photon Emission

Anael Ben-Asher,^{*} Antonio I. Fernández-Domínguez, and Johannes Feist

*Departamento de Física Teórica de la Materia Condensada and Condensed Matter Physics Center (IFIMAC),
Universidad Autónoma de Madrid, E28049 Madrid, Spain*

Single-photon sources are in high demand for quantum information applications. A paradigmatic way to achieve single-photon emission is through anharmonicity in the energy levels, such that the absorption of a single photon from a coherent drive shifts the system out of resonance and prevents absorption of a second one. We identify a novel mechanism for single-photon emission through non-Hermitian anharmonicity, i.e., anharmonicity in the losses instead of in the energy levels. We demonstrate the mechanism in two types of systems, including a feasible setup consisting of a hybrid metallodielectric cavity weakly coupled to a two-level emitter, and show that it induces high-purity single-photon emission at high repetition rates.

The generation and manipulation of nonclassical light are essential for light-based quantum information technologies [1]. Nonclassical light is characterized by photons that are correlated with each other, and therefore, their arrival times are dependent. The likelihood to detect coincident photons is usually quantified by the normalized high-order correlation functions at zero delay, $g_{\tau=0}^{(n \geq 2)}$ [2]. While $g_{\tau=0}^{(n)} = 1$ characterizes a coherent source of classical light with a Poissonian distribution of the photon arrival times, $g_{\tau=0}^{(n=2)} < 1$ characterizes a sub-Poissonian distribution associated with quantum light. When $g_{\tau=0}^{(n)} \ll 1$, the source can essentially only emit a single photon at a time. Such single-photon devices play a vital role in secure communications [3, 4], quantum computing [5–8], quantum metrology [9–11] and quantum sensing [12].

Single-photon emission can be generated by emitters that behave like two-level systems to a good approximation, such as atoms [13], nitrogen-vacancy (NV) centers in diamonds [14], and quantum dots [15]. While these inherently nonlinear systems offer a straightforward approach for single-photon emission, they have limitations in efficiency, emission rates, coherence time, and scalability [14, 16, 17]. As an alternative, cavity modes, which couple efficiently to light and are highly tunable, can potentially be used to achieve bright photon emission at high rates. However, they are inherently linear due to their bosonic nature, such that single-photon emission can only be achieved through physical mechanisms inducing an effective nonlinearity [18]. In this Letter, we describe a novel mechanism for generating efficient single-photon emission at high rates using cavity modes.

A prominent mechanism for the generation of single photons using cavity modes is the so-called photon blockade (PB, also known as conventional antibunching) [19–21] phenomenon, observed across various platforms, e.g., in cavity quantum electrodynamical (QED) [19, 20] and optomechanical [22, 23] systems. This mechanism is traditionally interpreted in terms of the eigenstates of the undriven Hermitian Hamiltonian, which describes the effect of the coherent coupling of the system components but does not describe the modification of these dynamics

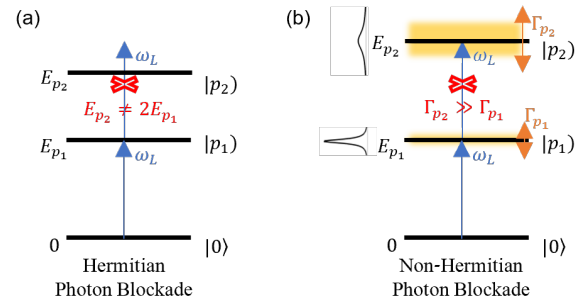


FIG. 1. Sketch of the two mechanisms for PB: (a) the Hermitian mechanism and (b) the NHPB mechanism introduced in this Letter.

due to losses. The anharmonicity of these eigenstates, i.e., the fact that the energy required to absorb one photon is different from the energy required to absorb a subsequent photon, induces the photon blockade effect. In contrast, the novel mechanism introduced in this Letter is based on the anharmonicity of the eigenstates of the effective undriven non-Hermitian (NH) Hamiltonian arising from the Lindblad master equation for open quantum systems [24, 25]. It becomes efficient when there is a significant difference in the losses (encoded in the imaginary parts of the NH eigenenergies) of the singly and doubly excited states of the system. Thus, we show that the effective NH Hamiltonian not only provides a mathematically convenient description including the effect of losses, but naturally points the way towards a non-Hermitian photon blockade (NHPB) mechanism. In this aspect, it is similar to phenomena such as exceptional points and parity-time symmetry that have attracted much attention in the last decade [26–35], and also arise naturally from a NH description.

Hermitian PB is difficult to realize in lossy systems, as the anharmonicity has to be larger than the linewidths (that are determined by the loss rates) of the system eigenstates [21], which is only achieved in the strong coupling regime of cavity QED systems. In contrast, NHPB is not limited by the linewidths but instead exploits their

possibly large values and operates in the weak-coupling regime of cavity QED systems, as we show below. The NHPB mechanism is thus expected to have less stringent experimental requirements than the Hermitian PB for the realization of an efficient single-photon source. Note that another antibunching mechanism, the destructive interference mechanism (also known as unconventional antibunching) [36–38] also usually operates in the weak-coupling regime; however, it suffers from severe limitations for single-photon generation [39].

We obtain a unified description of the PB phenomenon, which includes both the Hermitian and the NH mechanisms, using a perturbative approach to obtain a simple expression for the correlation functions under weak pumping by a continuous-wave source at frequency ω_L . The derivation details and the full expressions are given in the Supplemental Material [40]. In the common situation that only one eigenstate in each excitation manifold contributes significantly to the emission, the normalized zero-delay second-order correlation function $g_{\tau=0}^{(2)}$ is given by

$$g_{\tau=0}^{(2)}(\omega_L) \approx \left| \frac{\tilde{E}_{p_1} - \hbar\omega_L}{\frac{\tilde{E}_{p_2}}{2} - \hbar\omega_L} \right|^2 \frac{|(p_2|\hat{V}_p|p_1)|^2}{2|(p_1|\hat{V}_p|0)|^2} \times \frac{|(p_2|\mathbf{E}_D^-\mathbf{E}_D^-\mathbf{E}_D^+|p_2)|}{2|(p_1|\mathbf{E}_D^-\mathbf{E}_D^+|p_1)|^2} \quad (1)$$

where \hat{V}_p is the pumping operator that the external driving laser couples to, transformed into its rotating frame, \mathbf{E}_D^- is the scattered far-field operator at the detector, $|0\rangle$ is the ground state, and $|p_1\rangle$, $|p_2\rangle$ are the relevant eigenstates of the NH laser-free Hamiltonian in its first- and second-excitation manifolds. Their complex eigenenergies $\tilde{E}_j = E_j - \frac{i}{2}\Gamma_j$, where j can be either p_1 or p_2 , encode both the energy position E_j and loss rate Γ_j . Note that for eigenstates of a NH Hamiltonian, the notation $|\dots\rangle$, $\langle\dots|$ rather than $|\dots\rangle$, $\langle\dots|$ is used to describe the right and left eigenstates [41].

The emergence of both Hermitian and non-Hermitian PB manifests itself in the first row of Eq. (1), which presents the ratio between the populations of $|p_2\rangle$ and $|p_1\rangle$. In particular, the first term of Eq. (1) can be strongly suppressed when there is nonlinearity in the complex plane, i.e., when $\tilde{E}_{p_1} \neq \frac{\tilde{E}_{p_2}}{2}$. Fig. 1 shows a sketch of these two mechanisms: While the Hermitian PB in Fig. 1(a) stems from anharmonicity in the real axis $E_{p_1} \neq \frac{E_{p_2}}{2}$, the NHPB in Fig. 1(b) occurs even when $E_{p_1} = \frac{E_{p_2}}{2} = \hbar\omega_L$ and stems from the anharmonicity in the imaginary part of the eigenenergies. When the decay rate of $|p_2\rangle$ is much larger than that of $|p_1\rangle$, i.e., when $\Gamma_{p_2} \gg \Gamma_{p_1}$, as illustrated in Fig. 1(b), the state $|p_2\rangle$ is effectively eliminated from the dynamics such that the absorption of a second photon is prevented and $g_{\tau=0}^{(2)}(\omega_L)$ is strongly suppressed.

Note that the first term of Eq. (1) is the ratio between two Lorentzian functions centered at E_{p_1} and $E_{p_2}/2$ and whose widths are Γ_{p_1} and $\Gamma_{p_2}/2$, respectively. These Lorentzian functions are also depicted in Fig. 1(b). They represent the energy-dependent densities of states that correspond to $|p_1\rangle$ and $|p_2\rangle$ in the real energy spectrum and originate from their NH character [41]. This observation provides a physical explanation for the NHPB, revealing that the absorption of subsequent photons is suppressed due to a smaller density of states at twice the laser frequency than at the laser frequency itself.

As described above, realizing the NHPB mechanism requires a setup with a nonlinear behavior in losses. Specifically, the narrowest accessible eigenstates, i.e., those with the lowest losses, in each excitation manifold of the laser-free system are the relevant $|p_1\rangle$ and $|p_2\rangle$ which should obey $\Gamma_{p_1} \ll \Gamma_{p_2}$ to induce it. This points towards a way to design single-photon sources by engineering the loss of the levels in the system, instead of designing a specific energetic structure and trying to minimize losses as the Hermitian PB suggests. In the following, we theoretically demonstrate this concept and present the implementation of the NHPB mechanism through the engineering of losses by tailoring the coherent coupling between different modes with a given loss within the effective NH laser-free Hamiltonian framework. Note that this loss-engineering approach differs from actively designing the operators in the Lindblad master equation to modify the system's interaction with the environment states [42–45]. We present two examples where the necessary nonlinearity is induced by different effects. The first example is a proof-of-principle model with nonlinear coupling between linear elements that facilitates analytical analysis, while the second example presents a realistic system of a hybrid metallodielectric cavity interacting with a two-level emitter (TLE) in which the nonlinearity is due to linear coupling to a nonlinear system: a TLE.

The first example is a prototypical NH Hamiltonian describing second-harmonic generation [46],

$$\hat{H}_0 = \tilde{\omega}_a a^\dagger a + \tilde{\omega}_b b^\dagger b + g(a^\dagger b^2 + (b^\dagger)^2 a), \quad (2)$$

where a (a^\dagger) and b (b^\dagger) are the annihilation (creation) operators of two bosonic modes, $\tilde{\omega}_a = 2\omega_b - \frac{i}{2}\gamma_a$ and $\tilde{\omega}_b = \omega_b - \frac{i}{2}\gamma_b$ are their complex energies, and g is the quadratic coupling strength between them. Note that we have assumed that the real parts of the energies are exactly on two-photon resonance. This simple Hamiltonian can be analyzed analytically without any restriction to just a few eigenstates. In particular, when weakly pumping the b -mode ($\hat{V}_p = b^\dagger + b$) on resonance ($\omega_L = \omega_b$), and detecting its emission ($\mathbf{E}_D^- \propto b^\dagger$), the intensity I and the normalized zero-delay second-order correlation function $g_{\tau=0}^{(2)}$ are given by

$$I(\omega_L = \omega_b) \propto \frac{4}{\gamma_b^2}, \quad g_{\tau=0}^{(2)}(\omega_L = \omega_b) = \frac{1}{(1 + \eta)^2}, \quad (3)$$

where $\eta = \frac{4g^2}{\gamma_a\gamma_b}$ is the cooperativity parameter for the two modes [47]. $g_{\tau=0}^{(2)}(\omega_L = \omega_b)$ vanishes when $\eta \gg 1$. While large cooperativity can be obtained either through a large g , through a small γ_a , or through a small γ_b , the latter limit leads to the highest intensity and thus the most efficient single-photon emission. This limit corresponds exactly to the NHPB mechanism, while the limits of large g and small γ_a correspond to the Hermitian PB and the destructive interference mechanism, respectively. In the NHPB limit, the accessible first-excitation eigenstate $|p_1\rangle$, that is the pure b -mode with $\Gamma_{p_1} = \gamma_b$, is narrow. The second-excitation eigenstates, however, which arise from the interaction between the singly-excited mode a and the doubly-excited mode b , are much broader when $\gamma_b \ll \gamma_a$. In particular, when the coupling is weak ($g < \frac{\gamma_a}{2\sqrt{2}}$), the decay rate of the narrowest state $|p_2\rangle$ is given by $\Gamma_{p_2} \approx 2\gamma_b(1 + \eta)$. Thus, we obtain $g_{\tau=0}^{(2)}(\omega_L = \omega_b) \approx \left(\frac{2\Gamma_{p_1}}{\Gamma_{p_2}}\right)^2$, demonstrating the manifestation of the NHPB mechanism. In addition, to emphasize that the low two-photon emission given by $g_{\tau=0}^{(2)}(\omega_L = \omega_b)$ indicates the low two-photon absorption characterizing the NHPB, we note that the upconversion efficiency of two absorbed photons with frequency ω_b to one emitted photon with frequency $2\omega_b$, given by $\Phi_{up} = \frac{\eta}{\eta + \gamma_a/\gamma_b}$ (see [40] for details), is very small in the NHPB limit.

The Hamiltonian in Eq. (2) can, e.g., describe a mechanical oscillator (mode b) located exactly in the middle of a Fabry-Pérot cavity (mode a), when the optical mode is strongly driven by a laser (see Refs. [48–50]). Since commonly the mechanical decay rate is much smaller than the optical one [48–50], the NHPB induces single-phonon emission in such a system. For example, for $\frac{\gamma_b}{\gamma_a} = 10^{-3}$ and $g = \frac{\gamma_a}{10}$, the cooperativity is $\eta = 40$. Consequently, $g_{\tau=0}^{(2)}(\omega_L = \omega_b) \approx 6 \times 10^{-3}$ (Eq. (3)), showing strong antibunching. Note that adiabatic elimination of the mode a in Eq. (2) leads to a single oscillator with a nonlinear loss. Single-phonon emission in such a system has been demonstrated in Ref. [51].

The second example we discuss is a feasible cavity-QED-like setup involving the linear coupling of a TLE to bosonic (cavity) modes. In order to generate the anharmonicity in the complex plane that induces the NHPB, two bosonic modes with different losses are required. Hybrid metallodielectric cavities, incorporating a narrow photonic mode and a broad plasmonic mode, provide an excellent platform that fits this requirement. These cavities have attracted much attention lately, both theoretically [52–55] and experimentally [56–58], since they combine the merits of low-loss microcavities with highly localized plasmons, thus yielding new functionalities. Very recent works [59–62] have studied the photon statistics of a hybrid cavity coupled to a TLE and showed that it can present strong antibunching. These works related the antibunching to the destructive interference mechanism [59–61], and/or

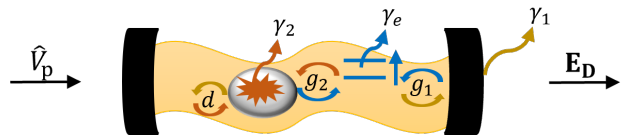


FIG. 2. Scheme of a hybrid metallodielectric cavity interacting with a TLE. The parameters characterizing the system are sketched. \hat{V}_p and \mathbf{E}_D describe the pumping of the Fabry-Pérot mode and the detection of its emission, respectively.

utilized large coupling strengths or energy detuning to induce the Hermitian PB mechanism [60–62]. In contrast, we here demonstrate that NHPB in such a system can lead to efficient single-photon emission without requiring large coupling strengths or energy detunings.

The NH Hamiltonian that describes the coupling between a TLE and two optical modes (e.g., a Fabry-Pérot mode and a plasmonic mode) can be written as

$$\hat{H}_0 = (\omega_e - i\frac{\gamma_e}{2})\sigma_+\sigma_- + \sum_{n=1,2} [(\omega_n - i\frac{\gamma_n}{2})a_n^\dagger a_n + g_n(\sigma_+ a_n + a_n^\dagger \sigma_-)] + d(a_1^\dagger a_2 + a_2^\dagger a_1). \quad (4)$$

Here, σ_- (σ_+) and a_n (a_n^\dagger) are the annihilation (creation) operators of the TLE and the two optical modes, respectively; ω_e, ω_n and γ_e, γ_n are respectively their energies and decay rates; g_1, g_2 are the coupling strengths between the TLE and each optical mode, and d is the coupling strength between the two optical modes originating from the interaction between the Fabry-Pérot electric field and the plasmonic dipole moment. Note that due to the non-Hermiticity of the system and the fact that the Hermitian and anti-Hermitian parts of the effective Hamiltonian do not commute, diagonalizing the Hermitian part to decouple the two optical modes would yield dissipative interactions. Consequently, there is no equivalent system of uncoupled bosonic modes that provides the same dynamics [63, 64]. In the following, we show the importance of the coupling d in inducing the NHPB mechanism. Without loss of generality, we assign index 1 to the narrow (Fabry-Pérot) mode and index 2 to the broad (plasmonic) mode, such that $\gamma_2 \gg \gamma_1$. In addition, we consider $\gamma_e \ll \gamma_{1,2}$, which describes a good emitter at low temperatures (e.g., see Ref. [65]). Fig. 2 depicts an illustration of the system.

The NHPB mechanism is induced in the system above by the decoupling of the Fabry-Pérot mode and emitter from the plasmonic mode occurring when $g_2, d \gg g_1, \gamma_e, \gamma_1$ [40]. This decoupling is only present in the first-excitation manifold, forming a very narrow $|p_1\rangle$. The state $|p_1\rangle$ resembles the dark state formed when several emitters interact with a cavity [66]. However, $|p_1\rangle$ is optically accessible by pumping the Fabry-Pérot mode and detecting its emission, such that $\hat{V}_p = a_1^\dagger + a_1$ and $\mathbf{E}_D \propto a_1^\dagger$. These operators describe a system configuration in which its

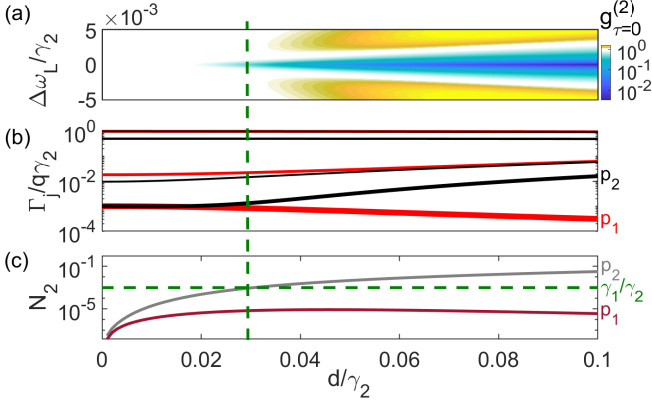


FIG. 3. (a) $g_{\tau=0}^{(2)}$ as a function of $\Delta\omega_L$, and d . (b) Γ_j/q of the first- (red, $q = 1$) and the second- (black, $q = 2$) excitation eigenstates and (c) $|(p_1|a_2^\dagger a_2|p_1)|$ (dark red) and $|(p_2|a_2^\dagger a_2|p_2)|$ (grey) as a function of d .

driving from and leakage into free space is mediated by the mirrors of the Fabry-Pérot cavity, as is presented in Fig. 2. Ref. [62] has discussed the formation of a very narrow $|p_1\rangle$ in a hybrid cavity interacting with a TLE and presented its role in enhancing the efficiency of the single-photon emission occurring due to the Hermitian PB mechanism. We here show that by engineering the decay rate of the narrowest state in the second-excitation manifold, $|p_2\rangle$, the very narrow $|p_1\rangle$ can be utilized to induce the NHPB mechanism.

The decay rate of $|p_2\rangle$ is engineered by controlling its plasmonic component. The plasmonic mode participates in $|p_2\rangle$ through its coupling d to the Fabry-Pérot mode. Fig. 3 studies the single-photon emission due to the NHPB mechanism with respect to d when $\gamma_1 = 10^{-3}\gamma_2$, $\gamma_e = 10^{-5}\gamma_2$, $g_1 = 0$, $g_2 = \frac{\gamma_2}{15}$ and $\omega_e = \omega_1 = \omega_2$. In Fig. 3(a), $g_{\tau=0}^{(2)}$ is shown as a function of the laser detuning $\Delta\omega_L = \omega_e - \omega_L$ and the coupling d , when pumping the Fabry-Pérot mode and detecting its emission. Note that, although not shown, the intensity reaches its maximum for $\Delta\omega_L = 0$ because the coupling strengths are sufficiently small not to induce Rabi splitting. The observed antibunching stems from the NHPB mechanism, i.e., from the anharmonicity in the imaginary part of the eigenenergies. This anharmonicity is presented in Fig. 3(b), which depicts the decay rates Γ_j of the first- (red) and second- (black) excitation eigenstates, normalized by the excitation number $q = 1, 2$, as a function of d . The decay rates of $|p_1\rangle$ and $|p_2\rangle$ are in thicker lines. Fig. 3(c) plots the plasmonic components of $|p_1\rangle$ (dark red line) and of $|p_2\rangle$ (grey line), given by $|(p_1|a_2^\dagger a_2|p_1)|$ and $|(p_2|a_2^\dagger a_2|p_2)|$, respectively, as a function of d . While the component of the plasmon in $|p_1\rangle$ is kept very small, consistent with its decoupling from $|p_1\rangle$, its component in $|p_2\rangle$ increases with larger d . When it reaches the ratio $\frac{\gamma_1}{\gamma_2}$ (dashed horizontal line in Fig. 3(c)), the decay rate of $|p_2\rangle$

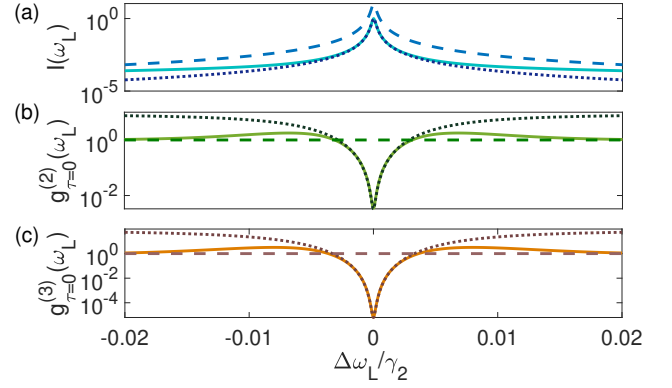


FIG. 4. (a) I , (b) $g_{\tau=0}^{(2)}$ and (c) $g_{\tau=0}^{(3)}$ as a function of $\Delta\omega_L$. The solid lines correspond to the full calculations [40], the dotted lines consider only the narrowest eigenstate in each excitation manifold, and the dashed lines were obtained when imposing $\Gamma_j = q\Gamma_{p_1}$ where q is the excitation number.

becomes significantly larger than that of $|p_1\rangle$ (Fig. 3(b)), inducing the emission of single photons (Fig. 3(a)).

Similarly to the previous example, $g_{\tau=0}^{(2)}$ can be expressed as a function of the cooperativity between the two optical modes $\eta = \frac{4d^2}{\gamma_1\gamma_2}$:

$$g_{\tau=0}^{(2)}(\omega_L = \omega_e) \approx \frac{1}{\eta^2} \left[\frac{g_2^2}{d^2} + 2 + 4 \left(\frac{g_2}{\gamma_2} \right)^2 \left(\frac{g_2^2}{d^2} - 1 \right) \right]^2, \quad (5)$$

showing that large η is required to achieve antibunching. Eq. (5) is the second-order approximation for the analytical expression of $g_{\tau=0}^{(2)}(\omega_L = \omega_e)$ when $\frac{\gamma_1}{\gamma_2} \ll 1$ and $\gamma_e = 0$. Further investigation of the dependence of the results and their robustness with respect to the system parameters is presented in the Supplemental Material [40].

Finally, in Fig. 4, we analyze the validity of the approximations inherent to our analysis above. Fig. 4(a) and Fig. 4(b) plot I and $g_{\tau=0}^{(2)}$, respectively, as a function of $\Delta\omega_L$ when $d = \frac{\gamma_2}{10}$ (and the other parameters are as in Fig. 3). In addition, since single-photon emission requires the suppression of all the high-order correlations $g_{\tau=0}^{(n)}$, we present in Fig. 4(c) the normalized zero-delay third-order correlation function $g_{\tau=0}^{(3)}$ as a function of $\Delta\omega_L$. The strong dip in Fig. 4(c) (solid line) demonstrates that the NHPB operates beyond second-order processes and suppresses multi-photon events. Moreover, the results support that the predicted antibunching is related to the generalized PB phenomenon and not to the destructive interference effect [39]. To verify that the predicted antibunching can be well-understood in terms of just two system eigenstates, $|p_1\rangle$ and $|p_2\rangle$, as Eq. (1) does, we compare I , $g_{\tau=0}^{(2)}$ and $g_{\tau=0}^{(3)}$ obtained by including all system eigenstates (solid lines) with the values obtained only by the narrowest eigenstates in each manifold, $|p_1\rangle$, $|p_2\rangle$ and $|p_3\rangle$ (dotted lines). As can be seen, almost perfect agreement is achieved between the two cases in the vicinity of

$\Delta\omega_L = 0$. Furthermore, we show that artificially setting all the eigenstates to have the same decay rate $\Gamma_j = q\Gamma_{p_1}$ (dashed lines) suppresses the antibunching completely. q is the excitation number, and Γ_{p_1} is the decay rate of $|p_1\rangle$. This suppression demonstrates that indeed the anharmonicity in the imaginary part of the eigenenergies, i.e., the NHPB mechanism, is the origin of the observed antibunching.

To conclude, we have theoretically proposed a novel mechanism for generating high-purity single-photon emission at high repetition rates. This mechanism stems from the difference in linewidth between the absorption of one photon and of two photons, and can be explained by the anharmonicity in the complex NH eigenenergy spectrum. Thus, the NHPB mechanism reveals an interesting interplay between non-Hermiticity of the system and quantum nonlinearity of the emitted light. Importantly, it provides a reliable route to single-photon emission even in the weak-coupling regime where couplings do not overcome losses. We have demonstrated the NHPB in two types of systems, including a feasible cavity-QED-like setup with realistic parameters, and showed that it indeed induces strong antibunching. Our findings open the door to the realization of new single-photon devices with potential applications in quantum information, communication and metrology.

This work has been funded by the Spanish Ministry of Science, Innovation and Universities-Agencia Estatal de Investigación through grants PID2021-126964OB-I00, PID2021-125894NB-I00, and CEX2018-000805-M (through the María de Maeztu program for Units of Excellence in R&D). We also acknowledge financial support from the Proyecto Sinérgico CAM 2020 Y2020/TCS-6545 (NanoQuCo-CM) of the Community of Madrid, from the European Research Council through grant ERC-2016-StG-714870 and from the European Union's Horizon Europe Research and Innovation Programme through agreement 101070700 (MIRAQLS) and No. 101034324 (CIVIS3i).

* anael.benasher@uam.es

- [1] J. L. O'Brien, A. Furusawa, and J. Vučković, Photonic quantum technologies, *Nature Photonics* **3**, 687 (2009).
- [2] R. Loudon, *The quantum theory of light*, 1st ed, Oxford University Press, Oxford, 143 (1973).
- [3] N. Gisin, G. Ribordy, W. Tittel, and H. Zbinden, Quantum cryptography, *Reviews of Modern Physics* **74**, 145 (2002).
- [4] V. Scarani, H. Bechmann-Pasquinucci, N. J. Cerf, M. Dušek, N. Lütkenhaus, and M. Peev, The security of practical quantum key distribution, *Reviews of Modern Physics* **81**, 1301 (2009).
- [5] E. Knill, R. Laflamme, and G. J. Milburn, A scheme for efficient quantum computation with linear optics, *Nature* **409**, 46 (2001).
- [6] P. Kok, W. J. Munro, K. Nemoto, T. C. Ralph, J. P. Dowling, and G. J. Milburn, Linear optical quantum computing with photonic qubits, *Reviews of Modern Physics* **79**, 135 (2007).
- [7] D. E. Chang, A. S. Sørensen, E. A. Demler, and M. D. Lukin, A single-photon transistor using nanoscale surface plasmons, *Nature Physics* **3**, 807 (2007).
- [8] I. Shomroni, S. Rosenblum, Y. Lovsky, O. Bechler, G. Guendelman, and B. Dayan, All-optical routing of single photons by a one-atom switch controlled by a single photon, *Science* **345**, 903 (2014).
- [9] V. Giovannetti, S. Lloyd, and L. Maccone, Quantum metrology, *Physical Review Letters* **96**, 010401 (2006).
- [10] V. Giovannetti, S. Lloyd, and L. Maccone, Advances in quantum metrology, *Nature Photonics* **5**, 222 (2011).
- [11] C. J. Chunnillall, I. P. Degiovanni, S. Kück, I. Müller, and A. G. Sinclair, Metrology of single-photon sources and detectors: a review, *Optical Engineering* **53**, 081910 (2014).
- [12] C. L. Degen, F. Reinhard, and P. Cappellaro, Quantum sensing, *Reviews of Modern Physics* **89**, 035002 (2017).
- [13] B. Darquié, M. P. Jones, J. Dingjan, J. Beugnon, S. Bergamini, Y. Sortais, G. Messin, A. Browaeys, and P. Grangier, Controlled single-photon emission from a single trapped two-level atom, *Science* **309**, 454 (2005).
- [14] I. Aharonovich, S. Castelletto, D. Simpson, C.-H. Su, A. Greentree, and S. Praver, Diamond-based single-photon emitters, *Reports on progress in Physics* **74**, 076501 (2011).
- [15] J. Stachurski, S. Tamariz, G. Callsen, R. Butté, and N. Grandjean, Single photon emission and recombination dynamics in self-assembled gan/aln quantum dots, *Light: Science & Applications* **11**, 114 (2022).
- [16] I. Aharonovich, D. Englund, and M. Toth, Solid-state single-photon emitters, *Nature Photonics* **10**, 631 (2016).
- [17] J. Lee, V. Leong, D. Kalashnikov, J. Dai, A. Gandhi, and L. A. Krivitsky, Integrated single photon emitters, *AVS Quantum Science* **2**, 031701 (2020).
- [18] P. Lodahl, S. Mahmoodian, and S. Stobbe, Interfacing single photons and single quantum dots with photonic nanostructures, *Reviews of Modern Physics* **87**, 347 (2015).
- [19] K. M. Birnbaum, A. Boca, R. Miller, A. D. Boozer, T. E. Northup, and H. J. Kimble, Photon blockade in an optical cavity with one trapped atom, *Nature* **436**, 87 (2005).
- [20] J. Fink, M. Göppl, M. Baur, R. Bianchetti, P. J. Leek, A. Blais, and A. Wallraff, Climbing the jaynes-cummings ladder and observing its nonlinearity in a cavity qed system, *Nature* **454**, 315 (2008).
- [21] A. Faraon, I. Fushman, D. Englund, N. Stoltz, P. Petroff, and J. Vučković, Coherent generation of non-classical light on a chip via photon-induced tunnelling and blockade, *Nature Physics* **4**, 859 (2008).
- [22] P. Rabl, Photon blockade effect in optomechanical systems, *Physical Review Letters* **107**, 063601 (2011).
- [23] K. Stannigel, P. Komar, S.J.M Habraken, S.D. Bennett, M. D. Lukin, P. Zoller, and P. Rabl, Optomechanical quantum information processing with photons and phonons, *Physical Review Letters* **109**, 013603 (2012).
- [24] P.M. Visser and G. Nienhuis, Solution of quantum master equations in terms of a non-hermitian hamiltonian, *Physical Review A* **52**, 4727 (1995).
- [25] R. Sáez-Blázquez, J. Feist, F. J. García-Vidal, and A.I. Fernández-Domínguez, Photon statistics in collective strong coupling: Nanocavities and microcavities, *Physical Review A* **98**, 013839 (2018).

- [26] M. Liertzer, L. Ge, A. Cerjan, A.D. Stone, H. E. Türeci, and S. Rotter, Pump-induced exceptional points in lasers, *Physical Review Letters* **108**, 173901 (2012).
- [27] A. Regensburger, C. Bersch, M.-A. Miri, G. Onishchukov, D. N. Christodoulides, and U. Peschel, Parity–time synthetic photonic lattices, *Nature* **488**, 167 (2012).
- [28] L. Chang, X. Jiang, S. Hua, C. Yang, J. Wen, L. Jiang, G. Li, G. Wang, and M. Xiao, Parity–time symmetry and variable optical isolation in active–passive-coupled microresonators, *Nature Photonics* **8**, 524 (2014).
- [29] Y. Sun, W. Tan, H.-q. Li, J. Li, and H. Chen, Experimental demonstration of a coherent perfect absorber with pt phase transition, *Physical Review Letters* **112**, 143903 (2014).
- [30] J. Doppler, A. A. Mailybaev, J. Böhm, U. Kuhl, A. Girschik, F. Libisch, T. J. Milburn, P. Rabl, N. Moiseyev, and S. Rotter, Dynamically encircling an exceptional point for asymmetric mode switching, *Nature* **537**, 76 (2016).
- [31] W. Chen, Ş. Kaya Özdemir, G. Zhao, J. Wiersig, and L. Yang, Exceptional points enhance sensing in an optical microcavity, *Nature* **548**, 192 (2017).
- [32] J. Zhang, B. Peng, Ş. K. Özdemir, K. Pichler, D. O. Krimer, G. Zhao, F. Nori, Y.-x. Liu, S. Rotter, and L. Yang, A phonon laser operating at an exceptional point, *Nature Photonics* **12**, 479 (2018).
- [33] C. Wang, X. Jiang, G. Zhao, M. Zhang, C. W. Hsu, B. Peng, A. D. Stone, L. Jiang, and L. Yang, Electromagnetically induced transparency at a chiral exceptional point, *Nature Physics* **16**, 334 (2020).
- [34] C. Wang, W. R. Sweeney, A. D. Stone, and L. Yang, Coherent perfect absorption at an exceptional point, *Science* **373**, 1261 (2021).
- [35] M. S. Ergoktas, S. Soleymani, N. Kakenov, K. Wang, T. B. Smith, G. Bakan, S. Balci, A. Principi, K. S. Novoselov, S. K. Ozdemir, *et al.*, Topological engineering of terahertz light using electrically tunable exceptional point singularities, *Science* **376**, 184 (2022).
- [36] T.C.H. Liew and V. Savona, Single photons from coupled quantum modes, *Physical Review Letters* **104**, 183601 (2010).
- [37] M. Bamba, A. Imamoğlu, I. Carusotto, and C. Ciuti, Origin of strong photon antibunching in weakly nonlinear photonic molecules, *Physical Review A* **83**, 021802(R) (2011).
- [38] A. Majumdar, M. Bajcsy, A. Rundquist, and J. Vučković, Loss-enabled sub-poissonian light generation in a bimodal nanocavity, *Physical Review Letters* **108**, 183601 (2012).
- [39] E. Zubizarreta Casalengua, J. C. López Carreño, F. P. Laussy, and E. d. Valle, Conventional and unconventional photon statistics, *Laser & Photonics Reviews* **14**, 1900279 (2020).
- [40] See Supplemental Material.
- [41] N. Moiseyev, *Non-Hermitian quantum mechanics* (Cambridge University Press, 2011).
- [42] J. F. Poyatos, J. I. Cirac, and P. Zoller, Quantum reservoir engineering with laser cooled trapped ions, *Physical Review Letters* **77**, 4728 (1996).
- [43] Z. Leghtas, S. Touzard, I. M. Pop, A. Kou, B. Vlastakis, A. Petrenko, K. M. Sliwa, A. Narla, S. Shankar, M. J. Hatridge, *et al.*, Confining the state of light to a quantum manifold by engineered two-photon loss, *Science* **347**, 853 (2015).
- [44] A. Lingenfelter, D. Roberts, and A. Clerk, Unconditional fock state generation using arbitrarily weak photonic nonlinearities, *Science Advances* **7**, eabj1916 (2021).
- [45] X. Su, J.-S. Tang, K. Xia, *et al.*, Nonlinear dissipation-induced photon blockade, *Physical Review A* **106**, 063707 (2022).
- [46] C. Sanchez Muñoz, G. Frascella, and F. Schlawin, Quantum metrology of two-photon absorption, *Physical Review Research* **3**, 033250 (2021).
- [47] H. Tanji-Suzuki, I. D. Leroux, M. H. Schleier-Smith, M. Cetina, A. T. Grier, J. Simon, and V. Vuletić, Interaction between atomic ensembles and optical resonators: Classical description, in *Advances in atomic, molecular, and optical physics*, Vol. 60 (Elsevier, 2011) pp. 201–237.
- [48] H. Xie, G.-W. Lin, X. Chen, Z.-H. Chen, and X.-M. Lin, Single-photon nonlinearities in a strongly driven optomechanical system with quadratic coupling, *Physical Review A* **93**, 063860 (2016).
- [49] Z.-Y. Li, G.-R. Jin, T.-S. Yin, and A. Chen, Two-phonon blockade in quadratically coupled optomechanical systems, in *Photonics*, Vol. 9 (MDPI, 2022) p. 70.
- [50] H. Xie, C.-G. Liao, X. Shang, Z.-H. Chen, and X.-M. Lin, Optically induced phonon blockade in an optomechanical system with second-order nonlinearity, *Physical Review A* **98**, 023819 (2018).
- [51] J. Li, C. Ding, and Y. Wu, Highly nonclassical phonon emission statistics through two-phonon loss of van der pol oscillator, *Journal of Applied Physics* **128**, 234302 (2020).
- [52] X. Yang, A. Ishikawa, X. Yin, and X. Zhang, Hybrid photonic–plasmonic crystal nanocavities, *ACS Nano* **5**, 2831 (2011).
- [53] P. Peng, Y.-C. Liu, D. Xu, Q.-T. Cao, G. Lu, Q. Gong, Y.-F. Xiao, *et al.*, Enhancing coherent light–matter interactions through microcavity-engineered plasmonic resonances, *Physical Review Letters* **119**, 233901 (2017).
- [54] B. Gurlek, V. Sandoghdar, and D. Martín-Cano, Manipulation of quenching in nanoantenna–emitter systems enabled by external detuned cavities: a path to enhance strong-coupling, *ACS Photonics* **5**, 456 (2018).
- [55] N. Thakkar, M. T. Rea, K. C. Smith, K. D. Heylman, S. C. Quillin, K. A. Knapper, E. H. Horak, D. J. Masiello, and R. H. Goldsmith, Sculpting fano resonances to control photonic–plasmonic hybridization, *Nano Letters* **17**, 6927 (2017).
- [56] M. Barth, S. Schietinger, S. Fischer, J. Becker, N. Nüsse, T. Aichele, B. Lochel, C. Sonnichsen, and O. Benson, Nanoassembled plasmonic-photonic hybrid cavity for tailored light–matter coupling, *Nano Letters* **10**, 891 (2010).
- [57] Y. Luo, M. Chamanzar, A. Apuzzo, R. Salas-Montiel, K. N. Nguyen, S. Blaize, and A. Adibi, On-chip hybrid photonic–plasmonic light concentrator for nanofocusing in an integrated silicon photonics platform, *Nano Letters* **15**, 849 (2015).
- [58] S. Cui, X. Zhang, T.-l. Liu, J. Lee, D. Bracher, K. Ohno, D. Awschalom, and E. L. Hu, Hybrid plasmonic photonic crystal cavity for enhancing emission from near-surface nitrogen vacancy centers in diamond, *ACS Photonics* **2**, 465 (2015).
- [59] S. Shen, J. Li, and Y. Wu, Quantum statistics engineering in a hybrid nanoparticle-emitter-cavity system, *Physical Review A* **105**, 063702 (2022).
- [60] Y.-W. Lu, J.-F. Liu, Z. Liao, and X.-H. Wang, Plasmonic-photonic cavity for high-efficiency single-photon blockade, *Science China Physics, Mechanics & Astronomy* **64**, 1

- (2021).
- [61] Y.-W. Lu, J.-F. Liu, R. Li, Y. Wu, H. Tan, and Y. Li, Single-photon blockade in quasichiral atom–photon interaction: simultaneous high purity and high efficiency, *New Journal of Physics* **24**, 053029 (2022).
- [62] Y.-W. Lu, W.-J. Zhou, Y. Li, R. Li, J.-F. Liu, L. Wu, and H. Tan, Unveiling atom-photon quasi-bound states in hybrid plasmonic-photonic cavity, *Nanophotonics* (2022).
- [63] S. Franke, S. Hughes, M. K. Dezfouli, P. T. Kristensen, K. Busch, A. Knorr, and M. Richter, Quantization of quasinormal modes for open cavities and plasmonic cavity quantum electrodynamics, *Physical Review Letters* **122**, 213901 (2019).
- [64] I. Medina, F. J. García-Vidal, A. I. Fernández-Domínguez, and J. Feist, Few-mode field quantization of arbitrary electromagnetic spectral densities, *Physical Review Letters* **126**, 093601 (2021).
- [65] D. Wang, H. Kelkar, D. Martin-Cano, D. Rattenbacher, A. Shkarin, T. Utikal, S. Götzinger, and V. Sandoghdar, Turning a molecule into a coherent two-level quantum system, *Nature Physics* **15**, 483 (2019).
- [66] J. del Pino, J. Feist, and F. J. Garcia-Vidal, Quantum theory of collective strong coupling of molecular vibrations with a microcavity mode, *New Journal of Physics* **17**, 053040 (2015).

Supplemental material for: Non-Hermitian Anharmonicity Induces Single-Photon Emission

Anael Ben-Asher, Antonio I. Fernández-Domínguez, and Johannes Feist
*Departamento de Física Teórica de la Materia Condensada and Condensed Matter Physics Center (IFIMAC),
 Universidad Autónoma de Madrid, E28049 Madrid, Spain*

DESCRIPTION OF THE CORRELATION FUNCTIONS USING THE SYSTEM EIGENSTATES AND EIGENENERGIES

The effective Hamiltonian in the rotating frame of a system pumped by the laser with pumping strength Ω and by the operator \hat{V}_p can be written as [1]

$$\hat{H}_{\text{eff}} = \Delta\hat{H}_0 + \Omega\hat{V}_p. \quad (\text{S1})$$

Here, $\Delta\hat{H}_0 = \hat{H}_0 - \hbar\omega_L\hat{N}$ where \hat{H}_0 is the NH Hamiltonian of the laser-free system, \hat{N} is a number operator that counts how many laser photons have been absorbed by the system, and ω_L is the laser frequency. The system's steady state $|\Psi_{ss}\rangle$ can be determined perturbatively in the low pumping regime ($\Omega \rightarrow 0$). Expanding the solution as a power series in Ω , $|\Psi_{ss}\rangle = \sum_{n=0} \Omega^n |\Psi_n\rangle$, and solving $\hat{H}_{\text{eff}}|\Psi_{ss}\rangle = 0$ [1] yields the following Born series:

$$|\Psi_{ss}\rangle = \sum_{n=0} \Omega^n \left(\frac{1}{\Delta\hat{H}_0} \hat{V}_p \right)^n |0\rangle \quad (\text{S2})$$

where $|0\rangle$ is the system's ground state. By using the spectral representation of $\Delta\hat{H}_0$, such that $\frac{1}{\Delta\hat{H}_0} = \sum_q \sum_{r_q=1}^{N_q} \frac{|r_q\rangle\langle r_q|}{E_{r_q} - q\hbar\omega_L}$, we reveal the contribution of the system's eigenstates $|r_q\rangle$ corresponding to the eigenenergies E_{r_q} . Here, q is the excitation number (the eigenvalue of \hat{N}) and N_q is the number of eigenstates in the q -excitation manifold. The c-product $(\dots|\dots)$ is used due to the system's non-Hermiticity [2]. The intensity and second-order correlation function are evaluated, respectively, using the first- and second- order Born series:

$$\begin{aligned} I(\omega_L) &= |\Omega|^2 \left| \sum_{i=1}^{N_1} \sum_{j=1}^{N_1} \frac{\langle 0|\hat{V}_p|i\rangle}{E_i - \hbar\omega_L} (i|\mathbf{E}_D^- \mathbf{E}_D^+|j) \frac{(j|\hat{V}_p|0)}{E_j - \hbar\omega_L} \right| \\ G_{\tau=0}^{(2)}(\omega_L) &= |\Omega|^4 \left| \sum_{m=1}^{N_2} \sum_{n=1}^{N_2} \sum_{i=1}^{N_1} \sum_{j=1}^{N_1} \frac{\langle 0|\hat{V}_p|i\rangle}{E_i - \hbar\omega_L} \frac{(i|\hat{V}_p|m)}{E_m - 2\hbar\omega_L} (m|\mathbf{E}_D^- \mathbf{E}_D^- \mathbf{E}_D^+ \mathbf{E}_D^+|n) \frac{(n|\hat{V}_p|j)}{E_n - 2\hbar\omega_L} \frac{(j|\hat{V}_p|0)}{E_j - \hbar\omega_L} \right| \end{aligned} \quad (\text{S3})$$

where \mathbf{E}_D^- is the scattered far-field operator at the detector. The normalized second-order correlation is given by $g_{\tau=0}^{(2)}(\omega_L) = \frac{G_{\tau=0}^{(2)}(\omega_L)}{[I(\omega_L)]^2}$ [3]. Eq. (1) in the main text is obtained when considering only one eigenstate in each excitation manifold, i.e., considering only the terms $j = i = p_1$, $n = m = p_2$ in Eq. (S3). $g_{\tau=0}^{(3)}(\omega_L)$, depicted in Fig. 4 (c) in the main text, is given by $\frac{G_{\tau=0}^{(3)}(\omega_L)}{[I(\omega_L)]^3}$ where $G_{\tau=0}^{(3)}(\omega_L) = \langle \Psi_{ss} | \mathbf{E}_D^- \mathbf{E}_D^- \mathbf{E}_D^- \mathbf{E}_D^+ \mathbf{E}_D^+ \mathbf{E}_D^+ | \Psi_{ss} \rangle$ is evaluated in a similar manner as $G_{\tau=0}^{(2)}(\omega_L)$ and $I(\omega_L)$.

THE UPCONVERSION EFFICIENCY IN THE SECOND HARMONIC GENERATION HAMILTONIAN

Considering the situation where two photons were absorbed simultaneously by the system described by the Hamiltonian in Eq. (2) in the main text and that is weakly pumped through the b -mode, their upconversion efficiency is given by:

$$\Phi_{up} = \frac{\langle \Psi_{ss} | a^\dagger a | \Psi_{ss} \rangle}{\langle \Psi_{ss} | a^\dagger a | \Psi_{ss} \rangle + \langle \Psi_{ss} | b^\dagger b^\dagger b b | \Psi_{ss} \rangle}. \quad (\text{S4})$$

$|\Psi_{ss}\rangle$ is the steady state given in Eq. (S2) for $\hat{V}_p = b^\dagger + b$, $\omega_L = \omega_b$ and the \hat{H}_0 given in Eq. (2) in the main text, $\langle\Psi_{ss}|a^\dagger a|\Psi_{ss}\rangle$ quantifies the number of photons emitted from the a -mode, and $\langle\Psi_{ss}|b^\dagger b^\dagger bb|\Psi_{ss}\rangle$ quantifies the amount of two photons that were emitted simultaneously from the b -mode and were not upconverted. The expression given in the main text, $\Phi_{up} = \frac{\eta}{\eta + \gamma_a/\gamma_b}$, is analytically derived using the second-order Born series for $|\Psi_{ss}\rangle$.

NON-HERMITIAN PHOTON BLOCKADE (NHPB) IN A HYBRID CAVITY INTERACTING WITH A TWO-LEVEL EMITTER (TLE)

Forming a narrow first-excitation eigenstate and a broad second-excitation eigenstate

The Hamiltonian in Eq. (4) in the main text is represented (when $\omega_e = \omega_1 = \omega_2$) in the first-excitation manifold by the matrix:

$$\underline{\underline{H}}^{(1)} = \begin{pmatrix} \omega_e - i\frac{\gamma_e}{2} & g_1 & g_2 \\ g_1 & \omega_e - i\frac{\gamma_1}{2} & d \\ g_2 & d & \omega_e - i\frac{\gamma_2}{2} \end{pmatrix} \quad (\text{S5})$$

and in the second-excitation manifold by the matrix:

$$\underline{\underline{H}}^{(2)} = \begin{pmatrix} 2\omega_e - i\frac{\gamma_e + \gamma_1}{2} & d & \sqrt{2}g_1 & g_2 & 0 \\ d & 2\omega_e - i\frac{\gamma_e + \gamma_2}{2} & 0 & g_1 & \sqrt{2}g_2 \\ \sqrt{2}g_1 & 0 & 2\omega_e - i\gamma_1 & \sqrt{2}d & 0 \\ g_2 & g_1 & \sqrt{2}d & 2\omega_e - i\frac{\gamma_1 + \gamma_2}{2} & \sqrt{2}d \\ 0 & \sqrt{2}g_2 & 0 & \sqrt{2}d & 2\omega_e - i\gamma_2 \end{pmatrix}. \quad (\text{S6})$$

The basis sets used to build $\underline{\underline{H}}^{(1)}$ and $\underline{\underline{H}}^{(2)}$ are $\{\sigma_+|0\rangle, a_1^\dagger|0\rangle, a_2^\dagger|0\rangle\}$ and $\{\sigma_+a_1^\dagger|0\rangle, \sigma_+a_2^\dagger|0\rangle, \frac{(a_1^\dagger)^2}{\sqrt{2}}|0\rangle, a_1^\dagger a_2^\dagger|0\rangle, \frac{(a_2^\dagger)^2}{\sqrt{2}}|0\rangle\}$, respectively. We study the photon statistics of the emission from the Fabry-Pérot mode, $\mathbf{E}_D^- \propto a_1$.

A very narrow first-excitation state $|p_1\rangle$ can be formed, even when d and g_2 are not negligible, while approximating $\gamma_e \approx \gamma_1 \approx 0$ in two edge cases: (i) when $g_1 \rightarrow 0$ and (ii) when $g_2 \approx d$. In these cases, $|p_1\rangle$ corresponds to the zeroth-order eigenvector: $\vec{v}_{p_1}^{(0)} = \tilde{N}(-d \ g_2 \ 0)^t$, such that the singly-excited state of the plasmonic mode $a_2^\dagger|0\rangle$ is decoupled. \tilde{N} is the normalization factor of $\vec{v}_{p_1}^{(0)}$. The correction to this eigenvector to first order in g_1 , γ_1 , and γ_e is

$$\vec{v}_{p_1}^{(1)} = \sum_{\pm} \frac{16(g_1(d^2 - g_2^2) + idg_2\frac{\gamma_1 - \gamma_e}{2})}{A_{\pm}\sqrt{d^2 + g_2^2}\sqrt{A_{\pm}^2 + 16(d^2 + g_2^2)}} \vec{v}_{\pm}^{(0)} \quad (\text{S7})$$

where $A_{\pm} = -i\gamma_2 \pm \sqrt{16(d^2 + g_2^2) - \gamma_2^2}$ and $\vec{v}_{\pm}^{(0)}$ are the other zeroth-order eigenvectors of $\underline{\underline{H}}^{(1)}$ when $\gamma_e \approx \gamma_1 \approx 0$ and $g_1 \rightarrow 0$. The correction $\vec{v}_{p_1}^{(1)}$ is negligible when the following conditions are fulfilled:

$$\begin{aligned} \frac{|\gamma_1 - \gamma_e|}{4} &\ll \frac{2(g_2^2 + d^2)}{\gamma_2} \\ g_1|d^2 - g_2^2| &\ll \frac{2(g_2^2 + d^2)^2}{\gamma_2}. \end{aligned} \quad (\text{S8})$$

This gives rise to the formation of a very narrow state $|p_1\rangle$. Note that similar to Eq. (5) in the main text, the first condition requires large cooperativity for the two optical modes $\eta = \frac{4d^2}{\gamma_1\gamma_2}$. These conditions were derived by assuming that $\sqrt{d^2 + g_2^2} \ll \frac{\gamma_2}{4}$ (weak-coupling regime) and $A_+ \approx -\frac{8i(d^2 + g_2^2)}{k_2}$.

Forming a broad second-excitation eigenstate whose emission can be detected requires the coupling of the doubly excited state $\frac{(a_1^\dagger)^2}{\sqrt{2}}|0\rangle$ with a mode that involves excitation of the plasmonic mode. This is achieved through the coupling d between the two optical modes. Fig. 3 in the main text demonstrates that with increasing d , the narrowest second-excitation state $|p_2\rangle$ becomes broad due to the increasing component of the plasmonic mode in it.

Robustness with respect to g_2

Fig. S1 studies the effect of g_2 on the antibunching presented in Fig. 3 and Fig. 4 in the main text, when $d = \frac{\gamma_2}{15}$ (and the other parameters are as in Fig. 3 in the main text). Fig. S1(a) and Fig. S1(b) present the intensity I and the normalized zero-delayed second-order correlation function $g_{\tau=0}^{(2)}$. Moreover, to present the effect of g_2 on the components in $|p_1\rangle$ and $|p_2\rangle$, Fig. S1(c) and Fig. S1(d) depicts the components of the Fabry-Pérot and the plasmonic modes, N_1 and N_2 , respectively, in $|p_1\rangle$ and $|p_2\rangle$ as a function of g_2 . In agreement with the above-mentioned zero-order eigenvector of $|p_1\rangle$, the dark red line in Fig. S1(c) shows that when g_2 is relatively small, the component of the Fabry-Pérot mode in $|p_1\rangle$ is negligible. As a result, since Fig. S1(a) and Fig. S1(b) presents the photon statistics of the emission from the Fabry-Pérot mode, the detection of the single-photon emission is prevented. Then, there is a range of values of g_2 for which the antibunching is robust. However, when g_2 becomes too large, the antibunching is suppressed (Fig. S1(b)). This suppression occurs because increasing g_2 , while keeping d constant, decouples the state $a_1^\dagger a_1^\dagger |0\rangle$ from the states that involve excitation of the plasmonic mode, as is shown by the grey line in Fig. S1(d). Consequently, $|p_2\rangle$ is narrow has small decay rate, preventing the NHPB mechanism. Fig. S2 investigates the interplay between g_2 and d and presents $g_{\tau=0}^{(2)}$ as a function of g_2 and d when $\omega_L = \omega_e$ (and the other parameters are as in Fig. S1). The minimal values of d that can be used to induce antibunching through the NHPB mechanism are depicted in Fig. S2 as a function of g_2 by the dotted line, derived when equating Eq. (5) in the main text to 1 when $\frac{d}{g_2} \rightarrow 0$.

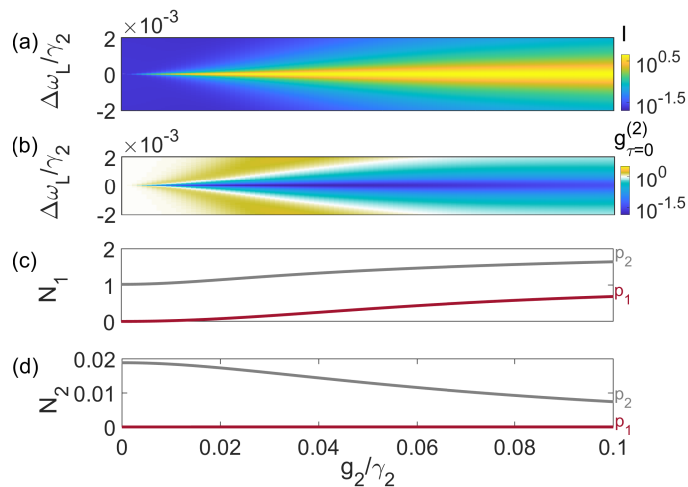


FIG. S1. (a) I and (b) $g_{\tau=0}^{(2)}$ as a function of $\Delta\omega_L = \omega_e - \omega_L$ and g_2 . (c) $N_1 = |(j|a_1^\dagger a_1|j)|$ and (d) $N_2 = |(j|a_2^\dagger a_2|j)|$, in $|p_1\rangle$ ($j = p_1$, dark red) and in $|p_2\rangle$ ($j = p_2$, grey) as a function of g_2 .

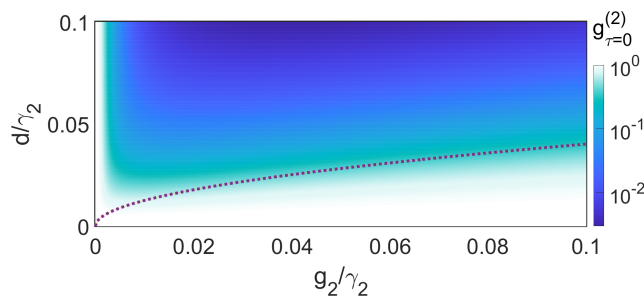


FIG. S2. $g_{\tau=0}^{(2)}$ as a function of d and g_2 . The dotted line corresponds to $d = (\frac{\gamma_1}{\gamma_2}(g_2^4 + \frac{g_2^2\gamma_2^2}{4}))^{\frac{1}{4}}$.

Robustness with respect to g_1

Fig. 3 in the main text presents the effect of increasing d on I and $g_{\tau=0}^{(2)}$, while g_1 is kept constant. However, when mode 1 and mode 2 are associated with the plasmonic and the Fabry-Pérot modes, respectively, g_1 is in principle proportional to d : while g_1 is given by the interaction of the Fabry-Pérot electric field with the TLE dipole moment μ_e , d is given by the interaction of the Fabry-Pérot electric field with the plasmonic dipole moment μ_2 . Consequently, when increasing the Fabry-Pérot electric field, both d and g_1 are increased with the fixed ratio $\frac{d}{g_1} = \frac{\mu_2}{\mu_e}$. Fig. S3 presents I and $g_{\tau=0}^{(2)}$ for this physical case, with all other parameters set to the same values as in Fig. 3 in the main text. Since g_1 is still smaller than d and the conditions in Eq. (S8) are fulfilled, Fig. S3 shows strong antibunching. The black and the red lines in Fig. S3(a) show, for each d , the pumping detuning that is required to populate $|p_1\rangle$ and $|p_2\rangle$, i.e., $\frac{E_{p1}-\omega_L}{\gamma_2}$ and $\frac{E_{p2}-\omega_L}{\gamma_2}$, where E_{p1} and E_{p2} are the real part of their eigenenergies. They show that Rabi splitting and emission in non-zero pumping detuning occur since g_1 reaches the strong-coupling regime for the TLE and the Fabry-Pérot mode.

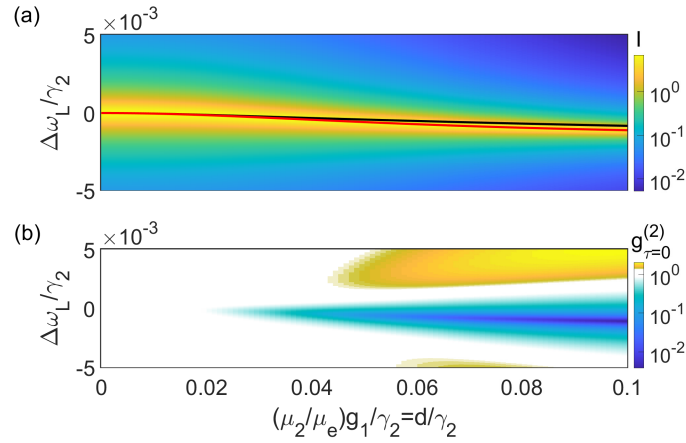


FIG. S3. (a) I and (b) $g_{\tau=0}^{(2)}$ as a function of $\Delta\omega_L = \omega_e - \omega_L$ and d , which is proportional to g_1 . The used ratio between d and g_1 is $\frac{\mu_2}{\mu_e} = 83.5$.

Robustness with respect to detuning the plasmonic mode

Fig. S4 studies the robustness of the antibunching presented in Fig. 3 and Fig. 4 in the main text when detuning the plasmonic mode from the TLE and Fabry-Pérot mode by δ_2 , i.e., when $\omega_2 = \omega_e + \delta_2$ in Eq. (4) in the main text. The other parameters are as in Fig. 4 in the main text. Fig. S4(a) shows $g_{\tau=0}^{(2)}$; Fig. S4(b) shows the decay rates of the first- (red) and second- (black) excitation eigenstates, where those of $|p_1\rangle$ and $|p_2\rangle$ are in thicker lines; and Fig. S4(c) shows the component of the plasmonic mode N_2 in $|p_1\rangle$ and $|p_2\rangle$. As can be seen from Fig. S4(a), the antibunching is robust for values of δ_2 that are smaller or comparable to the plasmonic decay rate γ_2 . Since the plasmonic mode is decoupled from $|p_1\rangle$ as is demonstrated by the dark red line in Fig. S4(c), its detuning affects only $|p_2\rangle$. The black line in Fig. S4(a) depicts for each value of δ_2 the pumping detuning that is required to populate $|p_2\rangle$, i.e., $\frac{\tilde{E}_{p2}-\omega_e}{\gamma_2}$, and shows that the detuning shifts the energy of $|p_2\rangle$. Consequently, the anharmonicity between $|p_1\rangle$ and $|p_2\rangle$ is not only in the imaginary part of their eigenenergies, shown in Fig. S4(b), but also in their real part. Therefore, the antibunching in Fig. S4(a) stems from both the Hermitian PB and the NHPB mechanisms. However, the anharmonicity is destroyed and the antibunching is suppressed for large values of δ_2 . The grey line in Fig. S4(c) shows that when δ_2 becomes too large, the plasmonic mode is decoupled not only from $|p_1\rangle$ but also from $|p_2\rangle$, forming a narrow $|p_2\rangle$ (thick black line in Fig. S4(b)) that prevents the occurrence of the NHPB mechanism.

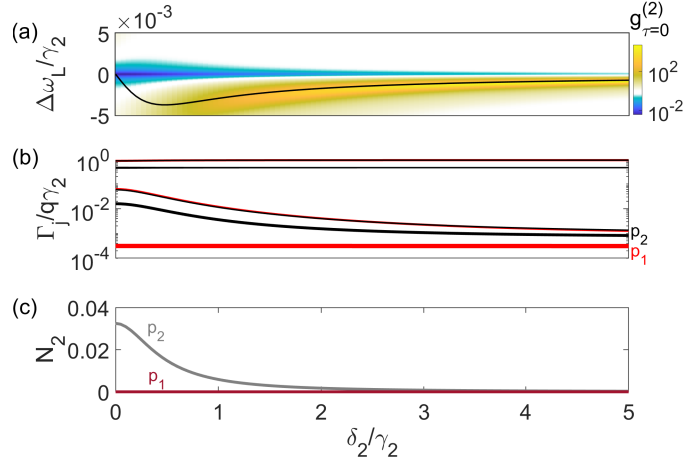


FIG. S4. (a) $g_{\tau=0}^{(2)}$ as a function of $\Delta\omega_L = \omega_e - \omega_L$ and $\delta_2 = \omega_2 - \omega$. (b) Γ_j/q of the first- (red, $q = 1$) and the second- (black, $q = 2$) excitation eigenstates as a function of δ_2 . (c) $N_2 = |(j|a_2^\dagger a_2|j)|$ in $|p_1\rangle$ ($j = p_1$, dark red) and in $|p_2\rangle$ ($j = p_2$, grey) as a function of δ_2 .

Robustness with respect to detuning the TLE

Fig. S5 studies the robustness of the antibunching presented in Fig. 3 and Fig. 4 in the main text when detuning the TLE from the optical modes by δ_e , i.e., when $\omega_e = \omega_1 + \delta_e$ ($\omega_1 = \omega_2$) in Eq. (4) in the main text. The other parameters are as in Fig. 4 in the main text. Fig. S5(a) shows I ; Fig. S5(b) shows $g_{\tau=0}^{(2)}$; and Fig. S5(c) shows the component of the plasmonic mode N_2 in $|p_1\rangle$ and $|p_2\rangle$. As can be seen from Fig. S5(b), the antibunching is robust when δ_e is relatively small but it is suppressed for larger values. Contrary to detuning the plasmonic mode (shown in Fig. S4), which is decoupled from $|p_1\rangle$, detuning the TLE affects both $|p_1\rangle$ and $|p_2\rangle$. Therefore, increasing δ_e shifts the pumping detuning that yields the maximal intensity (Fig. S5(a)) and the antibunching (Fig. S5(b)). Importantly, the dark red line in Fig. S5(c) shows that relatively large δ_e (that is larger by more than an order of magnitude than the Fabry-Pérot decay rate γ_1) destroys the decoupling of the plasmonic mode from $|p_1\rangle$, thus, forming a relatively broad $|p_1\rangle$. As a result, the NHPB mechanism and the antibunching are suppressed.

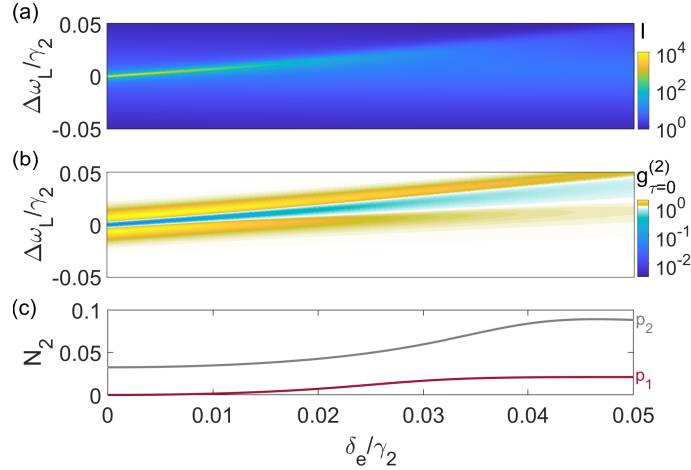


FIG. S5. (a) I and (b) $g_{\tau=0}^{(2)}$ as a function of $\Delta\omega_L = \omega_1 - \omega_L$ and $\delta_e = \omega_e - \omega_1$. (c) $N_2 = |(j|a_2^\dagger a_2|j)|$ in $|p_1\rangle$ ($j = p_1$, dark red) and in $|p_2\rangle$ ($j = p_2$, grey) as a function of δ_e .

-
- [1] R. Sáez-Blázquez, J. Feist, F. García-Vidal, and A. Fernández-Domínguez, Photon statistics in collective strong coupling: Nanocavities and microcavities, *Physical Review A* **98**, 013839 (2018).
 - [2] N. Moiseyev, *Non-Hermitian quantum mechanics* (Cambridge University Press, 2011).
 - [3] R. Loudon, *The quantum theory of light*, 1st ed, Oxford University Press, Oxford , 143 (1973).